Field ionization of Rydberg atoms in a single-cycle pulse

B. C. Yang and F. Robicheaux*

Department of Physics and Astronomy, Purdue University, West Lafayette, Indiana 47907, USA

(Received 5 March 2015; published 13 April 2015)

We study the ionization of Rydberg atoms in a single-cycle-pulse electric field based on both classical and quantum calculations. The ionization-probability curve exhibits a "ripple" structure as a function of the pulse duration and the field amplitude. These ripple structures are found to be dependent on the angular distribution of the initial state. A large electron-emission asymmetry is observed, and the ionized electron is almost completely emitted to one side of the atom except when the pulse length is roughly one Rydberg period. In both the long-pulse and the short-pulse regimes, larger electron energy can be expected from the ionization of lower-lying Rydberg states, matching the observation in a recent experiment [S. Li and R. R. Jones, Phys. Rev. Lett. **112**, 143006 (2014)]. This trend is closely related to the electron-emission asymmetry associated with the field-direction change in a single-cycle pulse. The possible implications of the different energy transfer in a single-cycle pulse from that in a multicycle pulse are also discussed briefly for the strong-field ionization of the ground atomic state.

DOI: 10.1103/PhysRevA.91.043407 PACS number(s): 32.60.+i, 32.80.Ee

I. INTRODUCTION

For the field ionization of Rydberg atoms in a static (or quasistatic) electric field, it has been well established that the required field amplitude $F_{10\%}$ for 10% ionization probability (which defines the field-ionization threshold) is proportional to n^{-4}, with n denoting the principal quantum number of the initial state. Recently, Li and Jones reported an experiment on the ionization of sodium Rydberg states in an intense single-cycle THz pulse [1], where the threshold field amplitude was found to deviate from this well-known scaling behavior, but follows a new relation: $F_{10\%} \propto n^{-3}$. Inspired by this observation, we have theoretically investigated the field-ionization threshold for both hydrogen and sodium atoms in a single-cycle pulse [2], and an empirical expression was obtained for the threshold behavior varying from the low-frequency limit to the short-pulse limit. When the pulse duration t_w becomes much shorter than one Rydberg period, the required threshold field amplitude is found to scale as $(n/t_w)^2$. A simple model that incorporates the nonzero displacement induced by a single-cycle pulse explains this threshold behavior.

In this paper, more detailed investigations are presented for the ionization of Rydberg atoms in a single-cycle-pulse electric field, including both the ionization probability and the electron energy spectra. Specifically, as in Refs. [1,2], a linearly polarized electric field is assumed to be along the z direction, which is considered as the pulse polarization direction, and its first half-cycle field is positive (along the z direction) with the second half-cycle field direction reversed. Oscillations are observed in the ionization-probability curves, which is a manifestation of the competition between the atomic Coulomb attraction and the spatial displacement induced by a single-cycle pulse. The effect induced by the spatial angular distribution of the initial state can be observed clearly in this kind of "ripple" structure, in contrast to the field-ionization threshold which was shown to be insensitive to different initial azimuthal quantum numbers [2].

A large asymmetry in the ionized-electron emission direction is observed after the single-cycle pulse, and its dependence on the pulse duration is investigated, as well as its connection with the associated energy spectra. The ionized electron always has a larger probability on the right side than that on the opposite side, where the right side is defined to be in the direction of the electric-field *force* acting on the electron by the *second* half-cycle field. Except when the pulse length is roughly one Rydberg period, the ionized electron is almost completely emitted to the right side. This is in contrast to the free-electron motion dressed by a single-cycle pulse, where the free electron must be shifted to the left side after the pulse. In particular, the ionized-electron wave on the right side is responsible for the high-energy part of the ionization spectrum, as well as the observed oscillatory structure in the spectrum.

The observation in Ref. [1] of larger electron energy obtained from the ionization of lower-lying Rydberg states is confirmed in our calculations for both hydrogen and sodium atoms. More importantly, the similar phenomenon can also be observed for the ionization of different bound states in the short-pulse regime. A simple explanation has been given in Ref. [1] based on an analog of the so-called "simple man" model [3–5]. The different energy-spectra ranges were attributed to the different ionization time of the electron from different Rydberg states during the interaction with a single-cycle pulse. In the present work, we are interested in the relationship between the ionization energy spectra and the electron-emission asymmetry associated with the change of the electric-field direction in a single-cycle pulse.

Furthermore, the energy transfer from a single-cycle pulse to an electron has been observed in Ref. [1] to be different from the standard prediction of the "simple man" model for a multicycle pulse [3–5]. For a multicycle pulse, the maximum energy transferred from the field to an electron is $2U_p$, which gives the cutoff of the ionization spectrum without back rescattering. U_p denotes the electron ponderomotive energy in an oscillating field. However, for a single-cycle pulse, the energy transfer can be larger than $6U_p$ for an electron ionized near the zero-field crossing point. Since this observation may be important for strong-field studies of ionization dynamics, the related theoretical issues are also addressed at the end of

*robichf@purdue.edu

this work by comparing the calculations for a single-cycle pulse with those for a three-cycle pulse.

The remainder of this paper is organized as follows. After briefly describing the theoretical model and the numerical methods in Sec. II, we investigate in Sec. III the nonlinear dependence of atomic ionization probability on the single-cycle pulse parameters. The electron-emission asymmetry is presented in Sec. IV, together with its manifestations in the ionization spectra. The possible implications of the different energy transfer in a single-cycle pulse from that in a multicycle pulse are discussed in Sec. V for the strong-field ionization of the ground atomic state. A brief conclusion is given in Sec. VI. Atomic units are used throughout this work unless specified otherwise.

II. THEORETICAL MODEL AND NUMERICAL METHODS

The applied single-cycle-pulse electric field $F(t)$ is assumed to be linearly polarized along the z direction. The corresponding Hamiltonian governing the electron motion can be written as

$$H = \frac{\mathbf{p}^2}{2} + V(r) + F(t)\cdot z, \tag{1}$$

where r is the radial coordinate of the electron relative to the nucleus, and $\mathbf{p}$ represents the electron momentum. The atomic potential is represented by $V(r)$. For hydrogen, $V(r) = -1/r$. A model potential as that in Ref. [2] is used for the sodium atom. The specific single-cycle pulse used in the present work has the following form:

$$F(t) = -C_0 F_m \left(\frac{t}{t_w}\right) e^{-[(\frac{t}{t_w})^2 + \frac{1}{10}(\frac{t}{t_w})^4]}, \tag{2}$$

where $C_0 = \sqrt{(\sqrt{35}+5)/5}\exp[(\sqrt{35}-4)/4]$ is a constant and is used to make the field-peak amplitude to be the value of F_m. This electric field gives a force on the electron that is in the negative z direction for $t < 0$ and is in the positive z direction for $t > 0$. We will use the shorthand "right side" to indicate positive z and "left side" for negative z.

The difference between the pulse profile in Eq. (2) and the amplitude-symmetric pulse we used in Ref. [2] is an added fourth-power term, $-(1/10)\cdot(t/t_w)^4$, on the exponential factor, which only brings a change in the exponential tail of the field profile. The reason we choose the pulse form in Eq. (2) is that it can make the numerical computation more efficient while still satisfying the zero-net-force condition for a real single-cycle pulse. As a comparison, by using the pulse profile in Ref. [2], the effective time interval should be $[-6t_w, 6t_w]$ for a practical numerical calculation. However, for the slightly modified profile in Eq. (2), the numerical simulation can be safely done in a shorter time interval $[-4t_w, 4t_w]$, beyond which the pulse field strength is negligibly small.

For numerically solving the time-dependent Shrödinger (TDS) equation, we consider the Hamiltonian in Eq. (1) as two parts: $H_1 = (\mathbf{p}^2)/2 + V(r)$ only containing the atomic part, and $H_2 = F(t)\cdot z$ representing the interaction term with an external single-cycle-pulse field. This separation scheme enables us to propagate the wave function on the radial dimension and the angular dimension independently by applying a split operator method [6,7]. The initial Rydberg state at $t = -4t_w$ is an eigenstate of H_1 with definite quantum number (n, l, m), which can be obtained by diagonalizing the H_1 matrix in a finite range $r < r_{\max}$ with a sufficiently large value of $r_{\max}$. Only the Rydberg states with $m = 0$ are considered in the present work. During the interaction with a linearly polarized single-cycle pulse, the instantaneous electron wave function can be represented as

$$\psi(\mathbf{r},t) = \sum_{l=0}^{l_{\max}} R_l(r,t) Y_{l0}(\theta,\phi) \tag{3}$$

on a two-dimensional (2D) space spanned by the discrete radial points and an angular momentum basis, where $\mathbf{r} = (r,\theta,\phi)$ denotes the electron coordinate relative to the nucleus and $R_l(r,t)$ represents the radial part of the electron wave function propagating on the radial dimension. The states with different l numbers in Eq. (3) are coupled by the applied single-cycle pulse through the interaction term H_2. For the propagation on the radial dimension, a Numerov approximation is adopted with a square-root mesh [7].

The final wave function ψ_f is recorded at $t = 4t_w$ when the single-cycle pulse is approximately zero. The surviving probability P_b for an electron still bound by the atomic Coulomb potential can be calculated by projecting ψ_f onto all the bound states which can be obtained by diagonalizing the atomic Hamiltonian H_1 in a large radial box $[0, r_{\max}]$. Therefore, the total ionization probability P is $(1 - P_b)$. For the longer pulses presented in Sec. III, a mask function such as that in Ref. [6] is used in the radial range $[(2/3)r_{\max}, r_{\max}]$ to absorb the ionized part approaching the numerical boundary.

The wave function $\psi_c(\varepsilon,\mathbf{r})$ for the ionized electron with positive energy ε can be obtained by projecting ψ_f onto all the continuum eigenstates $\varphi_{\varepsilon l0}$ of the atomic Hamiltonian H_1. Let $A_{\varepsilon l}$ denote the projection $\langle\varphi_{\varepsilon l0}|\psi_f\rangle$; then, the ionized-electron wave function $\psi_c(\varepsilon,\mathbf{r})$ has the following form:

$$\psi_c(\varepsilon,\mathbf{r}) = \sum_{l=0}^{l_{\max}} A_{\varepsilon l}\varphi_{\varepsilon l0}, \tag{4}$$

where each continuum state $\varphi_{\varepsilon l0}$ is energy normalized and is calculated by directly integrating the stationary Schrödinger equation with specific values of ε and l. The ionization spectra can be obtained from the ionized-electron wave function in Eq. (4). The total-energy spectrum is given by

$$\frac{dP}{dE} = \sum_{l=0}^{l_{\max}} |A_{\varepsilon l}|^2. \tag{5}$$

The left-side (right-side) energy spectrum is obtained from the outgoing-wave part of ψ_c at a large distance from the nucleus, by integrating the angular distribution over a half sphere with $z < 0$ ($z > 0$). For all the presented results in the following sections, the convergence is always checked with respect to the radial box $r_{\max}$, the angular-momentum boundary $l_{\max}$, the number of spatial points, the time step, and also the mask function if it is used.

In the three-dimensional classical trajectory Monte Carlo (3D CTMC) simulations, the classical Hamiltonian equations are propagated using a fourth-order Runga-Kutta algorithm

with adaptive time steps [8]. All of the trajectories are started from the outermost radial turning points which constitute an initial 3D sphere. The electron position on this initial sphere is selected according to the angular distribution of the initial quantum state, and its velocity direction is randomly selected on the tangent plane of the initial 3D sphere. The classical angular momentum is set to be $l + 0.5$. In order to mimic the electron radial distribution of the initial quantum state, for each trajectory propagation, we turn on the single-cycle-pulse electric field in Eq. (2) after a random time interval τ between zero and one Rydberg period, $T_{\rm Ryd} = 2\pi n^3$. We denote the field-turn-on time as $t = -4t_w$, i.e., the actual start time of each trajectory is $-4t_w - \tau$. The final energy E of each trajectory is recorded at $t = 4t_w$ when the single-cycle pulse is turned off.

The total ionization probability is obtained from the ratio of the number of trajectories with $E \geqslant 0$ to the total number of initially launched trajectories. The energy distribution $dP/dE = \Delta N/(N \cdot \Delta E)$, where ΔN denotes the number of trajectories with final energy falling in each discrete interval $[E_i - \Delta E/2, E_i + \Delta E/2]$. ΔE denotes the step size of the numerical energy points E_i, and N is the total number of trajectories in the simulations. After a sufficiently long propagation time, we track the velocity direction to determine the electron-emission asymmetry. A detailed discussion can be found in Ref. [9] about the possible small errors caused by different bins of initial trajectories. The accuracy of our present calculations is warranted by the comparison between classical and quantum results for both the ionization probability and the energy distribution.

III. "RIPPLE" STRUCTURE OF THE IONIZATION-PROBABILITY CURVE

For the ionization of atoms by different multicycle electric fields, various kinds of "ripple" structures (steps, bumps, or oscillations) have been observed before in the ionization-probability curves as a function of the applied field parameters. They are caused by different competing dynamical processes during the variation of the field parameters, including the nonsequential double ionization [10], different ionization thresholds [11,12], interplay between resonant and nonresonant multiphoton ionization processes [13], transition between the perturbative and the tunneling regimes [14,15], the phase-space metamorphoses, and nonlinear resonances [16,17].

For the present single-cycle pulse, there is a transition from the displacement ionization to the adiabatic above-the-barrier ionization when the pulse duration is increased from the short-pulse limit to the low-frequency limit [2]. Therefore, the possible ripple structure may also be expected in the

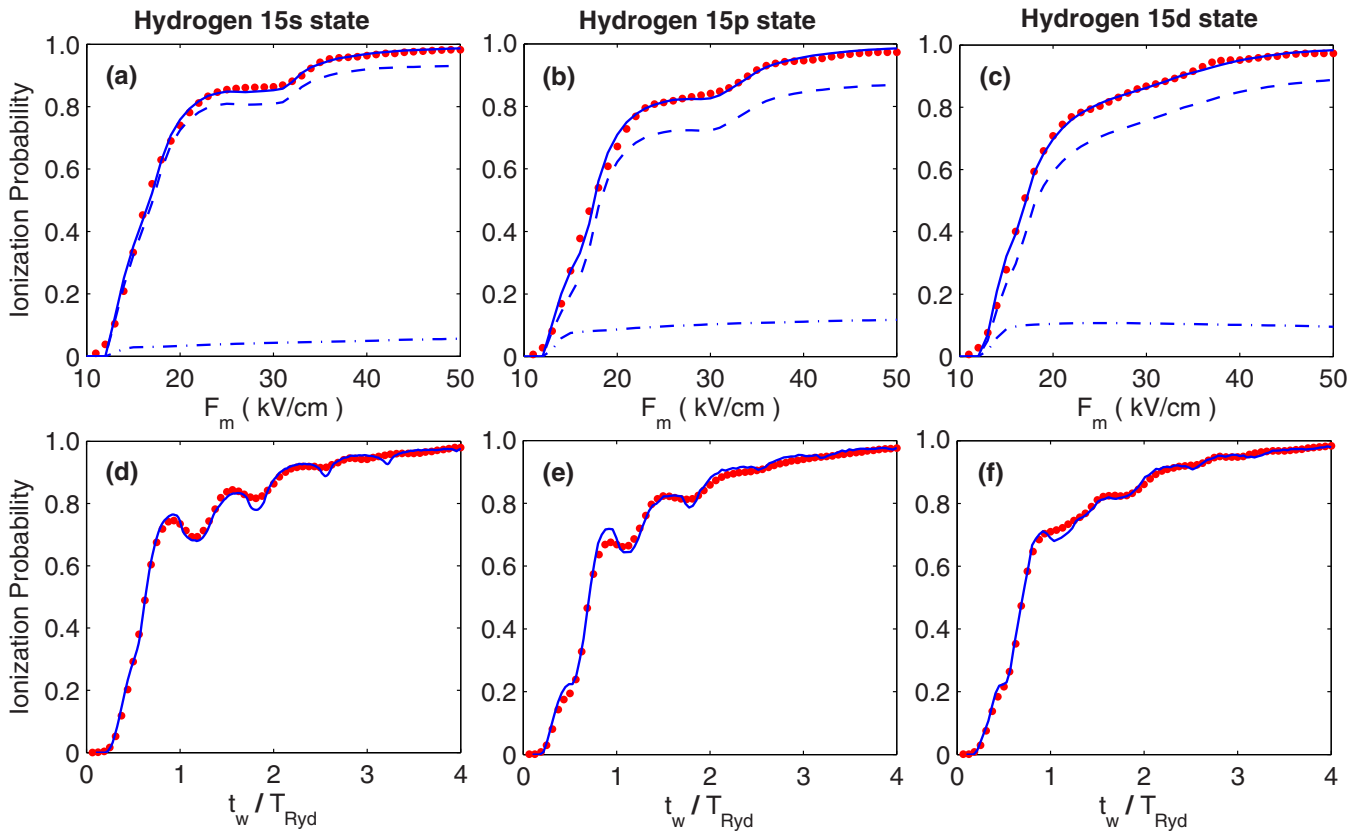

FIG. 1. (Color online) Ionization-probability curves as a function of the field parameters. (a)–(c) The ionization-probability curves as a function of the field amplitude for the hydrogen $15s$, $15p$, and $15d$ states, respectively, with $t_w = 0.5$ ps (approximately one Rydberg period). (d)–(f) The ionization-probability curves as a function of the pulse duration setting $F_m = 20$ kV/cm. The results from the CTMC simulation and solving the TDS equation are shown by the blue solid lines and the red solid circles, respectively, in each figure. The blue dashed and dot-dashed lines in (a)–(c) give the ionization probabilities from the CTMC simulation for the ionized electron emitted to the right side and that to the left side, respectively.

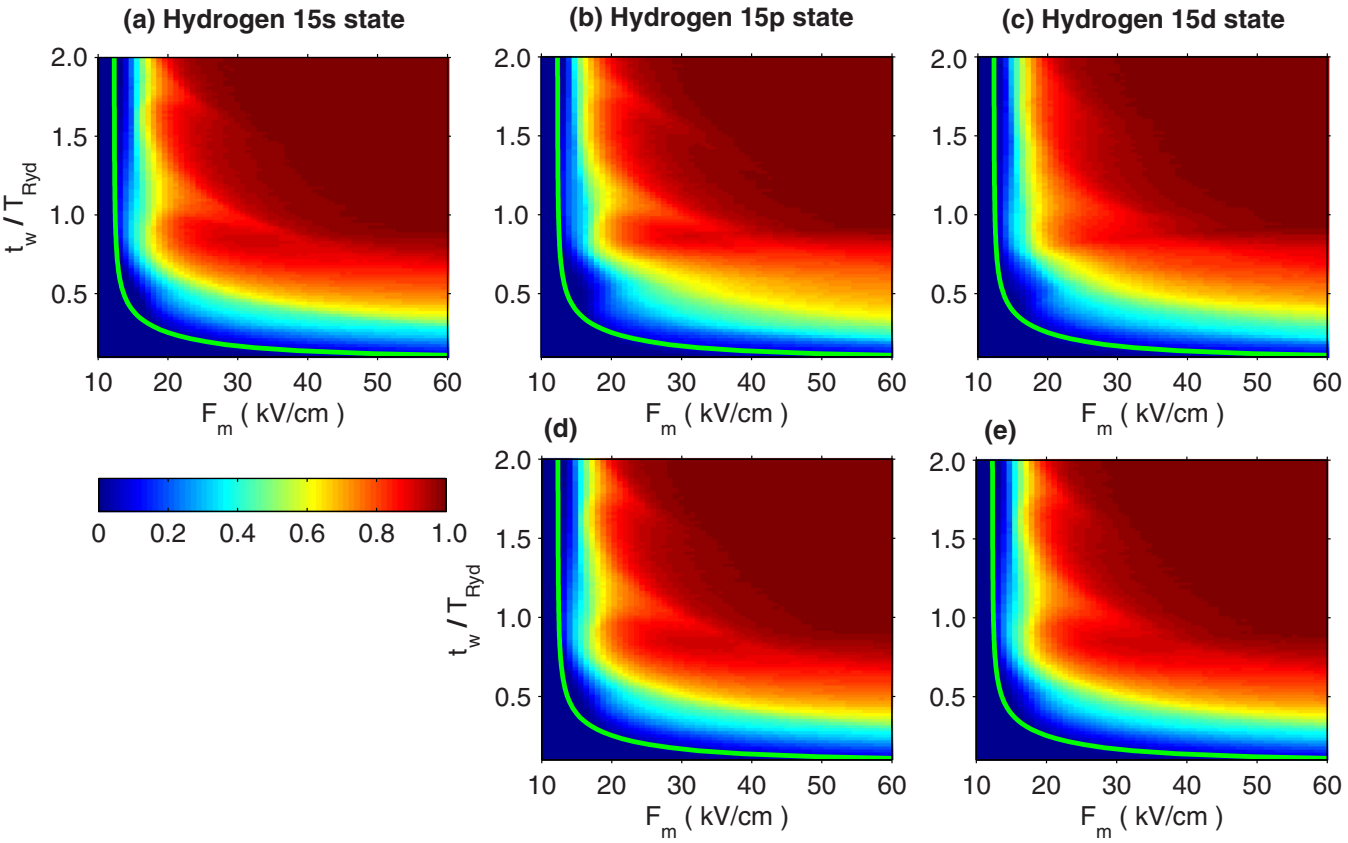

FIG. 2. (Color online) Landscape for the dependence of the ionization probability on the field parameters obtained from CTMC simulations. (a)–(c) Calculations for the hydrogen $15s$, $15p$, and $15d$ states, respectively. (d),(e) Results for the hydrogen $15p$ and $15d$ states, respectively, but using the same angular distribution as that for an s state. The values of ionization probabilities are indicated by a color bar on the left bottom. The green solid curve in each figure indicates the field-ionization threshold given by Eq. (6) in Ref. [2].

ionization-probability curve for the Rydberg-state ionization by a single-cycle pulse. The electron motion governed by the atomic Coulomb force will compete with the electron displacement caused by a single-cycle pulse in the middle regime where the electron can complete one or several orbits around the nucleus during the ionization process. In particular, since the action on the electron exerted by the single-cycle pulse is only in the z direction, the detailed dynamics of this competition is expected to be very different for the Rydberg orbits located at different angles relative to the pulse polarization direction.

The expected structures for the ionization-probability curves are shown in Fig. 1 by a comparison between calculations from the CTMC simulation and solving the TDS equation for hydrogen atoms. In Figs. 1(a)–1(c), $t_w = 0.5$ ps, approximately one Rydberg period for $n = 15$ ($T_{\rm Ryd} = 0.513$ ps). For the ionization-probability curve as a function of the applied field amplitude, a step structure can be observed clearly for $15s$ and $15p$ states, but is hardly observed for a $15d$ state. Besides this step structure, multiple oscillations are observed in the ionization-probability curve as a function of the single-cycle-pulse duration; Figs. 1(d)–1(f) are an example with $F_m = 20$ kV/cm. Again, the oscillations for a d state are much weaker than those for an s state or a p state. To get a whole vision of the dependence of ionization probability on both t_w and F_m, the variation of ionization probability is shown in Fig. 2 for the 2D parameter space spanned by $t_w/T_{\rm Ryd}$ and F_m. Figures 2(a)–2(c) display the CTMC-simulation results for the hydrogen $15s$, $15p$, and $15d$ states, respectively, where the ripple structures can be observed clearly, corresponding to the step structures in Figs. 1(a)–1(c) and the oscillations in Figs. 1(d)–1(f).

In contrast to the threshold behavior given by the green solid lines in Fig. 2 from Eq. (6) in Ref. [2], the detailed ripple structures of the ionization-probability curves are strongly dependent on the initial azimuthal quantum numbers. We attribute the differences among these ripple structures to the different angular distributions of Rydberg orbits associated with different l numbers. To confirm this expectation, a slightly modified CTMC simulation is made for the p and d states, where we use the same initial classical angular momentum $l + 0.5$ as that in Figs. 2(b) and 2(c), but turn off the different angular distributions: we use the same spherical-symmetric distribution as that for an s state. The obtained structures are displayed in Figs. 2(d) and 2(e) and are almost the same as that obtained for an s state in Fig. 2(a). This indicates that the different radial distributions with different l numbers have a negligible effect for the ripple-structure differences.

To get a picture of how electron orbits with different angles react to the single-cycle pulse, four representative cases are studied in Fig. 3 for the hydrogen $15s$ state. These calculations correspond to orbits with their outer turning points

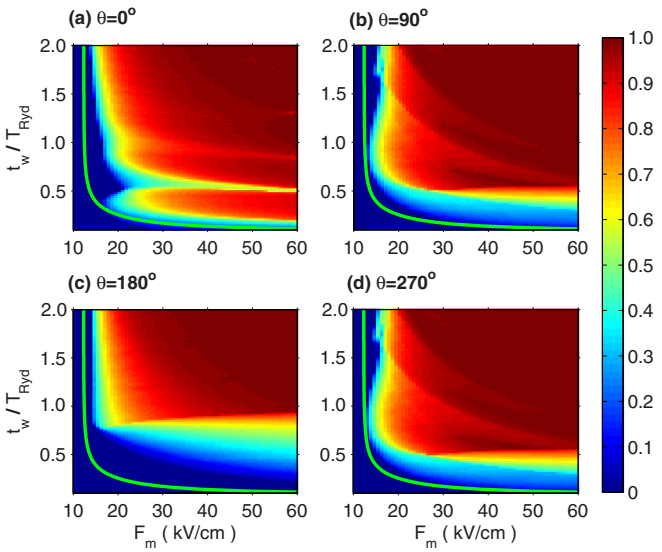

FIG. 3. (Color online) Dependence of the ionization probability on the field parameters obtained from CTMC simulations for individual Rydberg orbits from the hydrogen 15s state with different angles. (a) $\theta = 0°$, (b) $\theta = 90°$, (c) $\theta = 180°$, and (d) $\theta = 270°$ correspond to orbits with their outer turning points located, respectively, on the positive z axis, positive x axis, negative z axis, and negative x axis. The initial direction of the electron moving around the nucleus is always kept to be anticlockwise, and all of the orbits are in the xz plane. The color bar on the right shows the corresponding ionization-probability values, and the green solid curve in each figure indicates the ionization threshold given by Eq. (6) in Ref. [2].

located, respectively, on the positive z axis ($\theta = 0°$), positive x axis ($\theta = 90°$), negative z axis ($\theta = 180°$), and negative x axis ($\theta = 270°$). The electron direction around the nucleus is selected to be anticlockwise. The ionization probability is obtained from the same procedure as the CTMC simulation described in Sec. II. Figure 3 shows a strong dependence of the observed structure on the orbit's angle θ. The structures associated with the orbits of different angles in Fig. 3 can be qualitatively identified in Fig. 2 by looking at specific features near $t_w/T_{\rm Ryd} = 0.5$, 1.0, 1.5, and 2.0. These observations suggest that the angular distribution of the initial state plays an important role in the differences among those ripple structures in Figs. 1 and 2 for the hydrogen 15s, 15p, and 15d states.

IV. ELECTRON-EMISSION ASYMMETRY AND ENERGY SPECTRA

Electron-emission asymmetry along the field polarization direction (left-right asymmetry) has been studied extensively as a typical feature of strong-field ionization in a few-cycle pulse [18–20]. For the atomic ionization by a single-cycle pulse in the tunneling regime, the left-right asymmetry has been considered using simplified models based on the Landau-Dykhne approximation [21] or Keldysh-like theory [22]. The pulse-phase dependence of the left-right asymmetry has also been discussed for ionization of the hydrogen ground state based on both quantum and classical calculations [23]. For the Rydberg-state ionization considered here, a large asymmetry in the electron-emission direction is also expected as a result of the single-cycle nature of the applied field even though the ionization dynamics is in the barrier-suppression regime. We are mainly interested in the variation of the electron-emission asymmetry with different pulse lengths and its connection with the ionization spectra.

By varying the pulse duration as in Figs. 1(d)–1(f), the ionization-probability curves for the ionized electron on the side of the field-polarization direction (right side) and that on the opposite side (left side) are displayed, respectively, by the dashed and dot-dashed lines in Fig. 4 using a single-cycle pulse in Eq. (2) with $F_m = 20$ kV/cm. To measure the degree of the left-right asymmetry, an asymmetry parameter α_A is defined as [19]

$$\alpha_A = \frac{P_{\rm right} - P_{\rm left}}{P_{\rm right} + P_{\rm left}}, \tag{6}$$

with $P_{\rm right}$ and $P_{\rm left}$ denoting, respectively, the ionization probabilities for the ionized electron located on the right and the left sides. The electron-emission asymmetry is determined by tracking the final velocity direction of the ionized electron.

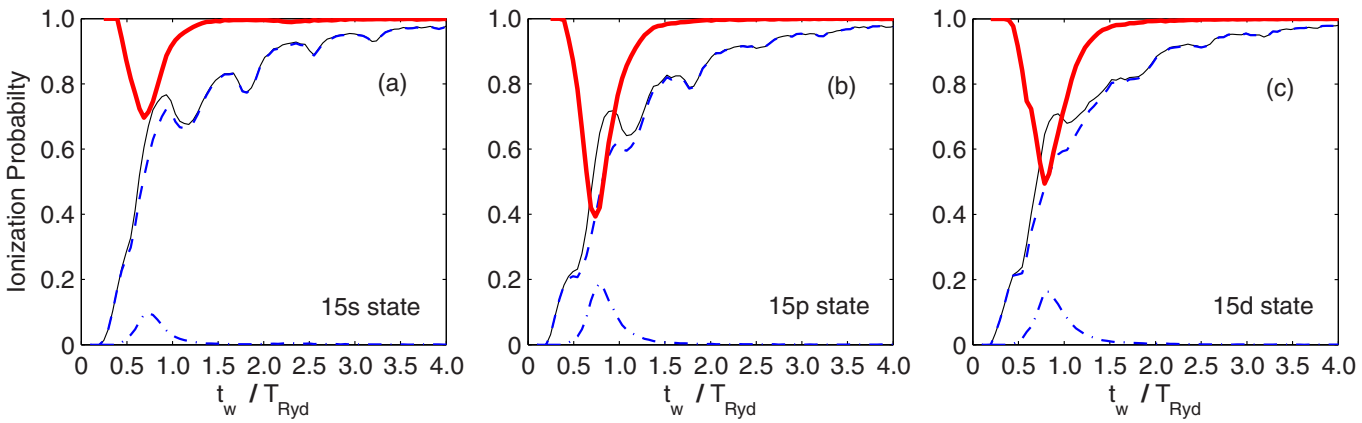

FIG. 4. (Color online) Dependence of the electron-emission asymmetry on the single-cycle pulse duration. (a)–(c) The hydrogen 15s, 15p, and 15d states, respectively. The thin black solid line shows the total ionization probability. The blue dashed and dot-dashed lines present the ionization probabilities for the electron emitted to the right side and to the left side, respectively. The asymmetry parameter α_A is given by the thick red solid line.

The asymmetry parameter α_A is always positive, irrespective of the pulse duration, as shown by the thick red solid curves in Fig. 4. This right-side preferred emission is different from that for a free electron. A free electron will be shifted to the left during the interaction with a single-cycle pulse given by Eq. (2). However, for an electron initially bound in an atom, a part of the energy transferred from the field is needed to offset the atomic binding energy during the ionization process. Assuming the electron is ionized in the first half cycle, the momentum in the left-side direction accumulated from the rest of the first half cycle will be less than the momentum in the right-side direction transferred from the second half cycle. Thus, the electron will tend to be directed to the right side. If the electron is ionized in the second half cycle, it will be directly ejected to the right side.

The simplified explanation in the previous paragraph ignored the Coulomb force after the time of ionization. The electron may also be scattered to the left side by interacting with the atomic Coulomb field. Since the pulse duration roughly determines how many times the scattering event can occur near the nucleus, the probability for the left-side electron emission as well as the asymmetry parameter α_A is expected to be dependent on the pulse duration. The curves of α_A have a dip when the pulse duration is roughly one Rydberg period, as shown in Fig. 4. Except for $t_w \sim T_{\rm Ryd}$, α_A approaches $+1$, meaning the electron is almost completely emitted to the right side. The details of the left-right asymmetry, such as the depth of the dip in Fig. 4, are also dependent on the angular distribution of the initial state.

In Figs. 1(a)–1(c), the ionization probabilities for the electron emitted to the left and the right sides are also displayed, respectively, by the dot-dashed and dashed lines, where the pulse duration $t_w = 0.5$ ps is approximately one Rydberg period ($T_{\rm Ryd} = 0.513$ ps for $n = 15$), and the left-side electron signal can be clearly observed (see Fig. 4). Besides the large electron-emission asymmetry, it can also be observed that the ripple structures of the total ionization-probability curves in Fig. 1 are mainly contributed by the ionized electron on the right side. The left-right asymmetry for other situations with different field strengths is also investigated. Two representative cases are shown in Fig. 5. Except for a shift of the dip-shape structure and its details, features similar to those in Fig. 4 are observed, though the electric-field strengths are much stronger than that used in Fig. 4.

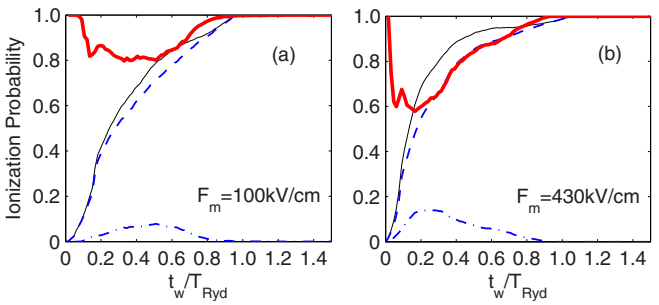

FIG. 5. (Color online) Electron-emission asymmetry for the hydrogen $15d$ state ionized by a stronger pulse field than that in Fig. 4. The field amplitude used in the CTMC simulation is indicated in each figure. The arrangement of different curves is the same as that in Fig. 4.

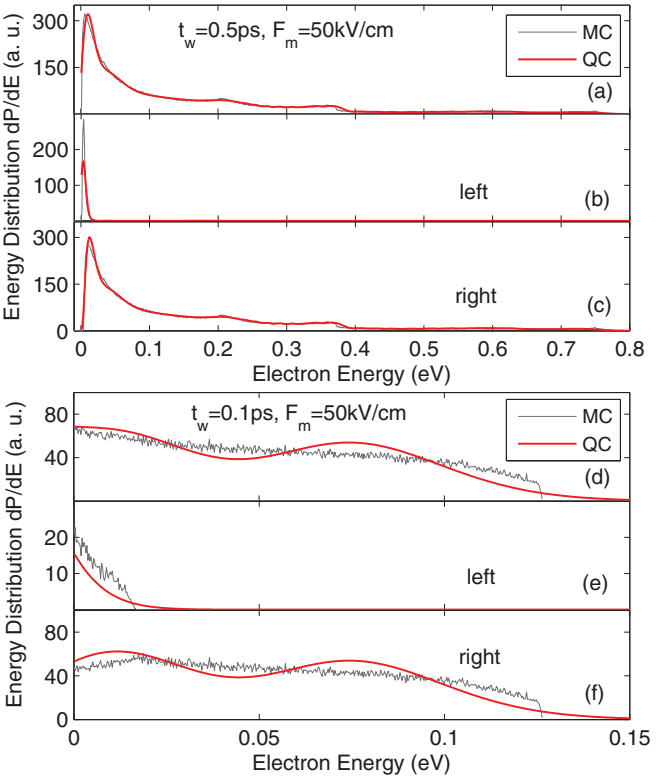

FIG. 6. (Color online) Electron energy spectra and left-right asymmetry for the hydrogen $15s$ state. The total ionization spectrum and the left-side and right-side ionization spectra are, respectively, displayed in order as (a)–(c) in the top panel ($F_m =$ 50 kV/cm, $t_w = 0.5$ ps) and (d)–(f) in the bottom panel ($F_m =$ 50 kV/cm, $t_w = 0.1$ ps). The thin gray curves present the CTMC-simulation results, while the thick red curves are calculated by solving the TDS equation. There are no adjustable parameters between the classical and the quantum results. The definition of the energy distribution dP/dE is the probability to find an electron per unit energy interval [20].

Following the above observations, it is interesting to explore the contributions of each-side emission in the final energy spectra. Two typical cases are shown in Fig. 6 for ionization of the hydrogen $15s$ state. First, it is demonstrated that structures observed in the energy spectra can be caused by both classical dynamics and quantum interferences. In the top panel of Fig. 6 with $t_w = 0.5$ ps (approximately one Rydberg period), quantum calculations almost coincide with CTMC simulations. Any effect from quantum interferences is hardly observed. This suggests that the observed structure in Figs. 6(a)–6(c) is mainly caused by classical dynamics. In contrast, in the bottom panel of Fig. 6 with $t_w = 0.1$ ps ($t_w/T_{\rm Ryd} \approx 0.2$), quantum oscillations can be observed clearly, while the background from classical dynamics appears smooth. Second, by recording the energy spectrum on each side (left and right), the results in Fig. 6 also indicate that both the classical and the quantum oscillations are dominantly contributed by the right-side emitted electron wave.

The other feature shown in Fig. 6 is that the energy-spectra range on the left side is much smaller than that on the right side. This large asymmetry of energy ranges is a direct result

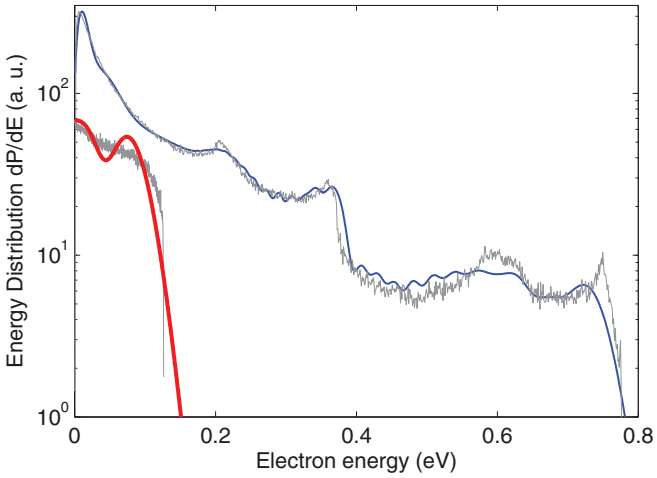

FIG. 7. (Color online) Comparison between the energy spectra from Figs. 6(a) and 6(d) on a logarithmic scale. The thin blue and thick red solid lines display the quantum spectra from Fig. 6(a) ($t_w = 0.5$ ps) and Fig. 6(d) ($t_w = 0.1$ ps), respectively. The corresponding spectra from CTMC calculations are shown by the thin gray curves.

induced by the second half cycle. Because its electric-field force acting on the electron is in the right-side direction, the second half cycle can accelerate the ionized electron to the right side and largely prevent the ionized electron from moving toward the left side. Furthermore, since a single-cycle pulse with $t_w = 0.5$ ps has a longer time during the second half cycle to accelerate the ionized electron in the right-side direction than a single-cycle pulse with $t_w = 0.1$ ps does, the maximum energy value in Fig. 6(a) turns out to be much larger than that in Fig. 6(d), which is shown more clearly in Fig. 7. The excellent agreement between quantum calculations and CTMC simulations in Figs. 6 and 7 further confirms the reliability of our CTMC-simulation scheme used in the present work.

It might be complicated to compare the energy-spectra ranges from the ionization of different Rydberg states, instead of the same initial state considered in Figs. 6 and 7. However, if most of the electron trajectories (in the framework of the CTMC simulation) have already been ionized at the end of the first half cycle, the situation should be predictable based on the following qualitative picture. During the first half cycle, the ionized electron is directed to the left side and gains momentum from the field. The momentum obtained by the ionized electron from a lower-lying state is smaller as a result of the larger atomic binding energy. During the second half cycle where the electric-field direction is reversed, the ionized electron will be stopped and then accelerated to the right side. The final momentum in the right-side direction is expected to be larger at the end of the second half cycle, if the ionized-electron momentum in the left-side direction is smaller at the end of the first half cycle. Therefore, the ionized electron from a lower-lying state can finally get a larger momentum in the right-side direction. Accordingly, the final kinetic energy of the ionized electron from a lower-lying state is expected to be larger, which is also the argument in Ref. [1], and corresponds directly to the experimental observation therein. Using a single-cycle pulse in Eq. (2) with $F_m = 430$ kV/cm and $t_w = 0.5$ ps, the final energy spectra for the sodium $6d$, $9d$,

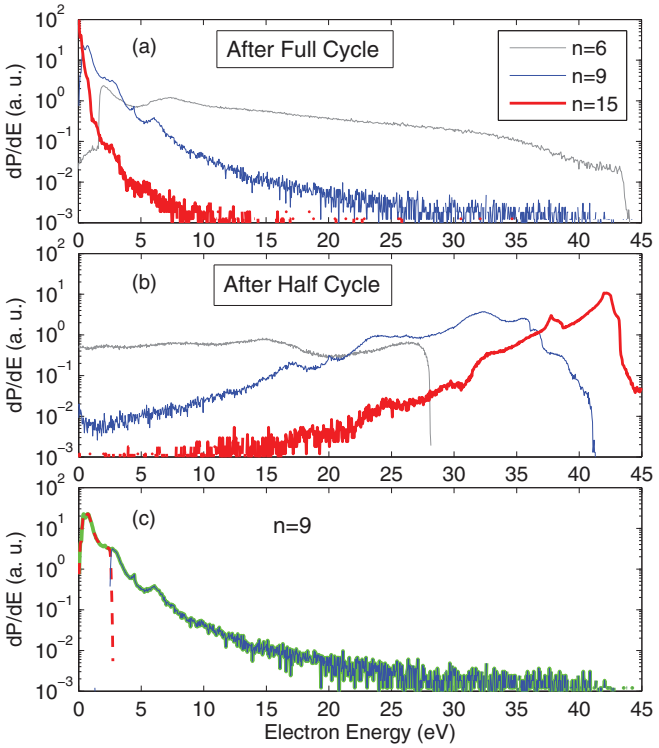

FIG. 8. (Color online) Comparison between the ionization spectra for sodium atoms in different bound states. A single-cycle pulse in Eq. (2) is used with $F_m = 430$ kV/cm and $t_w = 0.5$ ps (about one Rydberg period). The same model potential as that in Ref. [2] is adopted. (a) The final energy spectra after interacting with the full single-cycle pulse; (b) the ionization spectra at the end of the first half cycle. In both (a) and (b), the thick red curve, the blue curve, and the thin gray curve correspond to the CTMC-simulation spectra for the sodium $15d$, $9d$, and $6d$ states, respectively. The connection between the energy spectra in (a) and (b) is demonstrated in (c) by taking $n = 9$ as an example. The thick green curve in (c) is the full energy spectrum reproduced from (a). The evolution of electron trajectories with $E \geqslant 25$ and $0 \leqslant E < 25$ eV in (b) is tracked, and their final energy distributions after the full single-cycle pulse are displayed, respectively, by the red dashed curve and the thin blue solid curve in (c).

and $15d$ states are compared in Fig. 8(a), which confirms the experimental observation in Ref. [1]. The ionization spectra just after the first half cycle are also compared in Fig. 8(b), where the energy-spectra range from a low-lying state is smaller than that from a high-lying state.

The above dynamic picture can be demonstrated more clearly by looking at the evolution of the ionization spectrum from the end of the first half cycle to the end of the second half cycle. We take the sodium $9d$ state as an example, divide the ionization spectrum in Fig. 8(b) into two parts separated at $E = 25$ eV, and track the corresponding two groups of ionized trajectories until the end of the full single-cycle pulse. The final energy distributions of these two groups of ionized trajectories are displayed in Fig. 8(c), where the full curve of the ionization spectrum is also reproduced from Fig. 8(a) as a reference. Since the ionized trajectories with $0 \leqslant E < 25$ eV in Fig. 8(b) have smaller momenta in the left-side direction compared to those having $E \geqslant 25$ eV in Fig. 8(b), their final momenta

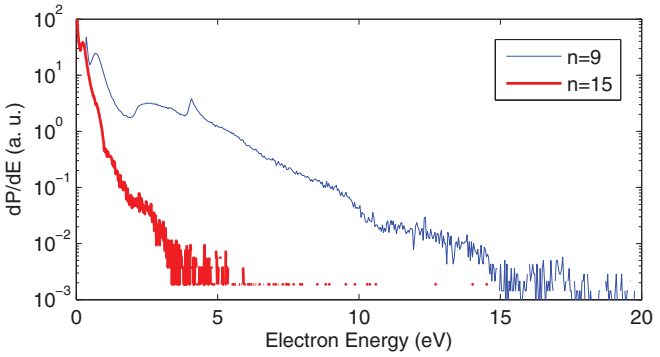

FIG. 9. (Color online) Comparison between the ionization spectra for hydrogen atoms in different bound states. The same field parameters as those in Fig. 8 are used. The thick red curve and the thin blue curve correspond to the CTMC-simulation spectra for the hydrogen $15d$ and $9d$ states, respectively. No ionization signal is obtained for the hydrogen $6d$ state because the ionization threshold is higher than the field amplitude used here (430 kV/cm).

will be larger after reversed to the right-side direction by the second half-cycle electric field. Consequently, their energy distribution will go to a higher-energy range at the end of the full single-cycle pulse, as shown by the thin blue solid curve in Fig. 8(c).

The ionization spectra for the hydrogen $9d$ and $15d$ states are compared in Fig. 9, where the similar phenomenon as that for sodium atoms in Fig. 8 can also be observed. Note that the electron cannot be ionized from the hydrogen $6d$ state by the single-cycle pulse with $F_m = 430$ kV/cm. In particular, the similar phenomenon associated with the energy spectra can also occur in the short-pulse regime. An example calculation is presented in Fig. 10 for the hydrogen $6d$, $9d$, and $15d$ states, where a single-cycle pulse with $t_w = 2.5$ fs and $F_m = 0.0198$ a.u. is applied. The peak intensity is about 2.7×10^{15} W/cm^2, corresponding to the scaled field strength $F_m n^4 = 1000$ a.u. for $n = 15$. All of the ionized trajectories at the end of the first half cycle are tracked in our simulations until the end of the full cycle, as are their contributions to the final energy spectra. The evolution of the ionized trajectories is qualitatively consistent with the above dynamic picture.

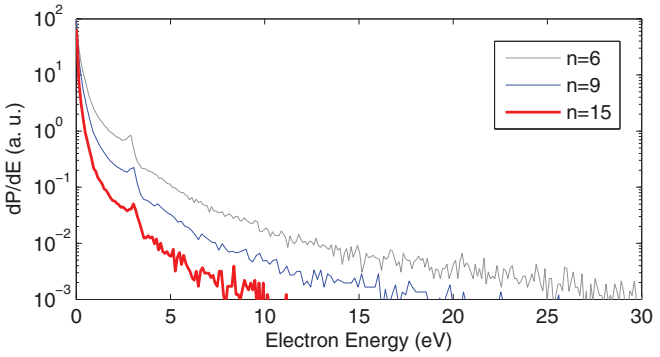

FIG. 10. (Color online) Same as Fig. 9 but in the short-pulse regime. A single-cycle pulse in Eq. (2) is used with $t_w = 2.5$ fs and a peak intensity of 2.7×10^{15} W/cm^2. The thick red curve, the blue curve, and the thin gray curve correspond to the CTMC-simulation spectra for the hydrogen $15d$, $9d$, and $6d$ states, respectively.

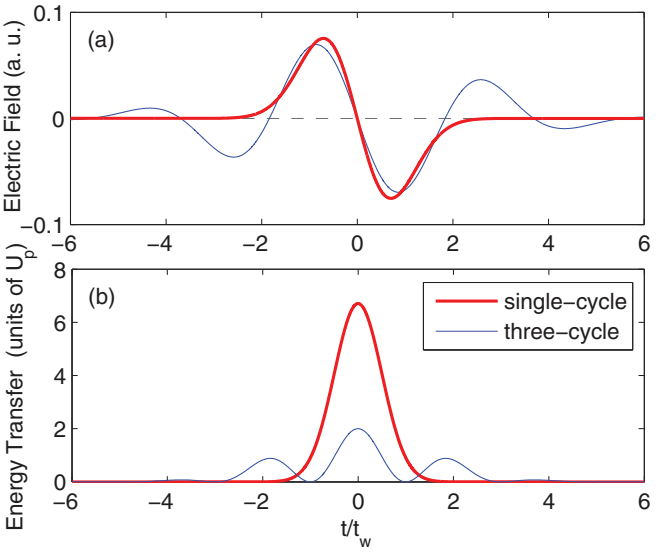

FIG. 11. (Color online) Comparison of a single-cycle pulse (thick red lines) with an approximate three-cycle pulse (thin blue lines). The field profile and the energy transfer from the field to an electron are compared in (a) and (b), respectively. The single-cycle pulse and the three-cycle pulse are given by Eqs. (7) and (8), respectively, with $t_w = 30$ a.u. and $F_m = 0.075$ a.u.

V. IMPLICATIONS FOR THE STRONG-FIELD IONIZATION OF THE GROUND ATOMIC STATE

An important observation in Ref. [1] is that the momentum (or energy) transfer from a single-cycle pulse to an electron is not consistent with the usual results of a "simple man" model for the strong-field ionization of ground-state atoms in a multicycle pulse. The vector-potential behavior of a single-cycle pulse is different from that of a multicycle pulse (see Fig. 11 for an example). However, according to the "simple man" model [3–5], the vector potential plays a critical role in determining the details of ionization dynamics. Therefore, an obvious difference should be expected between the strong-field ionization in a multicycle pulse and that in a true single-cycle pulse. As a limiting case of the few-cycle pulse, there have been discussions of the strong-field ionization in a single-cycle pulse, including both one-electron ionization [21–26] and double ionization [27–29]. However, the differences between the vector potential in a single-cycle pulse and that in a multicycle pulse have received little attention.

To address this issue directly, we first consider a specific single-cycle pulse in Fig. 11 generated by the following vector potential from Ref. [2]:

$$A(t) = -\frac{F_m t_w}{\sqrt{2}} e^{-(\frac{t}{t_w})^2+\frac{1}{2}}, \tag{7}$$

where $t_w = 30$ a.u. and $F_m = 0.075$ a.u., corresponding to a peak intensity of 2×10^{14} W/cm^2. The ionized-electron kinetic-energy spectrum is obtained in Fig. 12(d) for the hydrogen ground state by solving the TDS equation. It can be observed that the energy range extends to a value over $6U_p$ with its profile having a peak at about $2U_p$, where the "ponderomotive" energy $U_p = \frac{F_m^2}{4\omega^2}$ with $\omega = \frac{2\pi}{4t_w}$. A similar

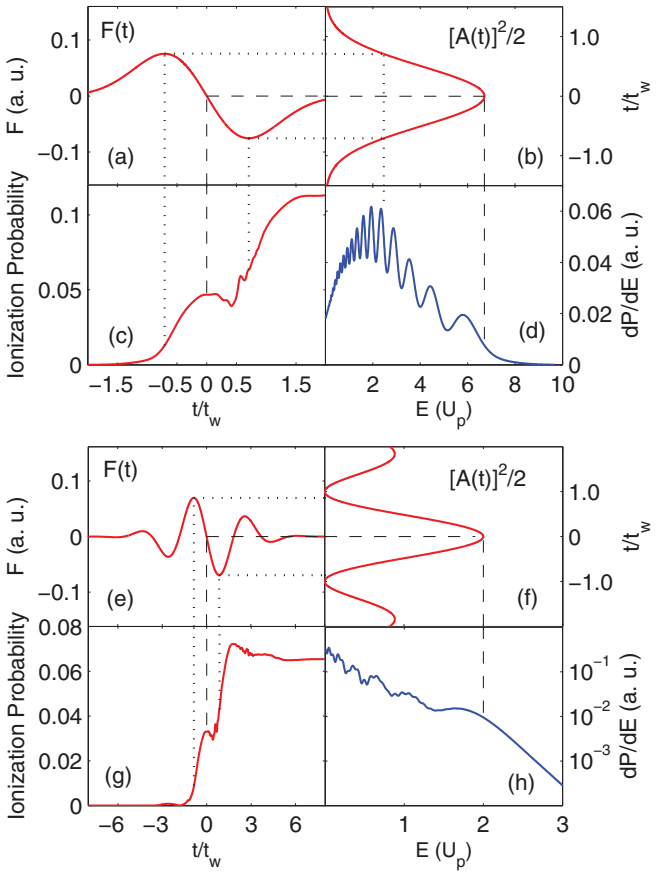

FIG. 12. (Color online) Strong-field ionization of the hydrogen ground state. The detailed field profile, the energy transfer from the field to an electron, the time-dependent ionization probability, and the final energy spectrum, respectively, for (a)–(d) a single-cycle pulse and (e)–(h) an approximate three-cycle pulse. The correspondences between different quantities are indicated by the dotted and the dashed lines for the central one cycle. The single-cycle pulse and the three-cycle pulse used in this figure are the same as those compared in Fig. 11.

profile with this peak structure appeared in a paper by Lerner, LaGattuta and Cohen in 1994 [27], and the related discussions about the interference oscillations, such as those in Fig. 12(d), can also be found in Ref. [26], but the connection with the special vector potential for a single-cycle pulse was not discussed.

To understand the structure of this spectra profile, the value of $[A(t)]^2/2$ is plotted in Fig. 12(b). This corresponds to the energy transfer observed in the experiment [1], and gives the final kinetic energy of an electron tunneling out with zero velocity at time t. The ionization probability is also recorded in Fig. 12(c) as a function of time. Near the field-peak position, the ionization rate is largest, and the electron tunneling out around this time can get a final energy of about $2U_p$ [Fig. 12(b)], which explains the observed peak around $2U_p$ in the spectra profile in Fig. 12(d). This correspondence is indicated by the dotted lines in Figs. 12(a)–12(d). As indicated by the dashed lines, the spectra range is determined by the maximum energy transfer near the zero-field crossing point where the ionization rate is small.

As a comparison, an approximate three-cycle pulse is considered, and is generated by the following vector potential:

$$A(t) = -(F_m/\omega)e^{-t^2/(3t_w)^2}\cos(\omega t), \tag{8}$$

where F_m, t_w, and ω are the same as those for the single-cycle pulse in Eq. (7). The three-cycle pulse, the energy transfer $[A(t)]^2/2$, the time-dependent ionization probability, and the final energy spectra are shown, respectively, in Figs. 12(e)–12(h), where the correspondences between the peak (or the cutoff) of the energy-spectra profile and different variables in Figs. 12(e)–12(g) are also indicated by the dotted lines (or the dashed lines). As is well known, the spectra profile for this kind of multicycle pulse always decreases monotonically with a cutoff at about $2U_p$, as shown in Fig. 12(h). The back rescattering of the electron with the rest ion is not considered here, which can extend the energy range to a much larger value, but with a much lower order.

From the comparison in Fig. 12, it can be found that although the ionization dynamics for the approximate three-cycle pulse is mainly confined in the central one cycle, as those observed before in the experiment [30], the energy transfer during the interaction and also the final energy spectrum are very different from those for a true single-cycle pulse, which is largely affected by the details of the vector potential. To be clear, the three-cycle pulse in Eq. (8) and its corresponding values of $[A(t)]^2/2$ are compared in Fig. 11 with those for the single-cycle pulse given by Eq. (7). It is obvious that the vector potentials are different between a multicycle pulse and a true single-cycle pulse, though the field profiles are almost the same in the central one cycle.

Although Eqs. (7) and (8) are used, respectively, to express the vector potentials for a single-cycle pulse and a multicycle pulse, the differences presented in Figs. 11 and 12 are actually independent of the choice of specific expression for the vector potential. Equation (8) can also give a single-cycle pulse like that we used above by setting the pulse duration short enough relative to the carrier-wave period $(2\pi/\omega)$. However, in the single-cycle-pulse limit, as a result of the much shorter duration of the pulse envelope relative to the carrier-wave period, the field parameters of the expression in Eq. (8), especially the carrier-wave frequency ω, lose their physical meanings as those that they hold for a multicycle pulse.

The last point we would like to stress is that the above situation we considered is in the regime where the quasistatic approximation can still be applied. If the pulse duration t_w in Eq. (7) becomes smaller gradually, the quasistatic approximation will break down. The corresponding peak structure as that in Fig. 12(d) may disappear in the spectra profile, and the diabatic response of the electron to an applied short single-cycle pulse can be expected in the ionization dynamics.

VI. CONCLUSION

Inspired by a recent experiment on the field ionization of low-lying sodium Rydberg states in an intense single-cycle pulse [1], and also based on our previous study of the field-ionization threshold behavior in the short-pulse limit [2], we presented detailed investigations of the ionization dynamics in

a single-cycle pulse. A linearly polarized pulse is considered with its first half-cycle field along a positive-z direction and the second half-cycle field inverted. As a result of the competition between the Coulomb attraction from atomic nucleus and the spatial displacement induced by a single-cycle pulse, "ripple" structures can be observed in the ionization-probability curve as a function of the pulse duration and the field amplitude, which was shown to be dependent on the angular distribution of the initial state.

A large electron-emission asymmetry was observed after the single-cycle pulse. The ionized electron is preferably emitted to the positive-z direction (right side). The left-side emission can only be observed clearly when the pulse length is roughly one Rydberg period of the initial state. The right-side emitted electron contributes to both the classical and the quantum structures in the energy spectra, and is also responsible for the high-energy part of the ionization spectra. As observed in the experiment [1], the ionized electron from a low-lying state can reach a larger energy range than that from a high-lying state, even in the short-pulse regime. Although the calculations presented in this work are mainly for Rydberg atoms, the observed phenomena are also expected for strong-field ionization of much lower bound states in the barrier-suppression ionization regime.

The manifestations of the different vector-potential behaviors between a single-cycle pulse and a multicycle pulse were also discussed for the strong-field ionization of the ground atomic state in the tunneling-ionization regime. Both the energy range and the general profile of the ionization spectrum in a single-cycle pulse are different from those in a multicycle pulse. We showed that the ionization dynamics in a multicycle pulse is quite different from that in a true single-cycle pulse, even if the ionization mainly occurs during the central one cycle of the multicycle pulse. The momentum transfer from the field to an electron is determined by the details of the vector potential. Since short-pulse techniques are rapidly developing [31,32], the phenomena discussed above could be investigated by experiments in the near future.

ACKNOWLEDGMENTS

This work was supported by the U.S. Department of Energy, Office of Science, Basic Energy Sciences, under Award No. DE-SC0012193. We thank Professor C. H. Greene and Professor R. R. Jones for helpful discussions. B.C.Y. appreciates the stimulating discussions with Dr. Chen Zhang, Dr. Antonio Picon Alvarez, Dr. Hua-Chieh Shao, Changchun Zhong, Su-Ju Wang, and Yijue Ding.

[1] S. Li and R. R. Jones, Phys. Rev. Lett. **112**, 143006 (2014).
[2] B. C. Yang and F. Robicheaux, Phys. Rev. A **90**, 063413 (2014).
[3] H. B. van Linden van den Heuvell and H. G. Muller, in *Multiphoton Processes*, edited by S. J. Smith and P. L. Knight (Cambridge University Press, Cambridge, 1988).
[4] T. F. Gallagher, Phys. Rev. Lett. **61**, 2304 (1988).
[5] P. B. Corkum, N. H. Burnett, and F. Brunel, Phys. Rev. Lett. **62**, 1259 (1989).
[6] T. Topçu and F. Robicheaux, J. Phys. B **40**, 1925 (2007).
[7] F. Robicheaux, J. Phys. B **45**, 135007 (2012).
[8] W. H. Press, B. P. Flannery, S. A. Teukolsky, and W. T. Vetterling, *Numerical Recepies in C* (Cambridge University Press, New York, 1988).
[9] F. Robicheaux, Phys. Rev. A **56**, 3358(R) (1997).
[10] B. Walker, B. Sheehy, L. F. DiMauro, P. Agostini, K. J. Schafer, and K. C. Kulander, Phys. Rev. Lett. **73**, 1227 (1994).
[11] D. R. Mariani, W. van de Water, P. M. Koch, and T. Bergeman, Phys. Rev. Lett. **50**, 1261 (1983).
[12] P. Pillet, H. B. van Linden van den Heuvell, W. W. Smith, R. Kachru, N. H. Tran, and T. F. Gallagher, Phys. Rev. A **30**, 280 (1984).
[13] X. M. Tong, Z. X. Zhao, and C. D. Lin, J. Phys. B **36**, 1121 (2003).
[14] S. Geltman, J. Phys. B **33**, 1967 (2000).
[15] C. Arendt, D. Dimitrovski, and J. S. Briggs, Phys. Rev. A **76**, 023423 (2007).
[16] J. E. Bayfield, S. Y. Luie, L. C. Perotti, and M. P. Skrzypkowski, Phys. Rev. A **53**, 12(R) (1996); L. C. Perotti, *ibid.* **81**, 033407 (2010).
[17] P. M. Koch and K. A. H. Leeuwen, Phys. Rep. **255**, 289 (1995).
[18] G. G. Paulus *et al.*, Nature (London) **414**, 182 (2001).
[19] A. Gürtler, F. Robicheaux, W. J. van der Zande, and L. D. Noordam, Phys. Rev. Lett. **92**, 033002 (2004).
[20] D. B. Milošević, G. G. Paulus, D. Bauer, and W. Becker, J. Phys. B **39**, R203 (2006), and references therein.
[21] V. S. Rastunkov and V. P. Krainov, J. Phys. B **40**, 2277 (2007); Laser Phys. **19**, 813 (2009); see also a comment in Ref. [22].
[22] B. M. Karnakov, V. D. Mur, S. V. Popruzhenko, and V. S. Popov, Phys. Lett. A **374**, 386 (2009).
[23] J. P. Hansen, J. Lu, L. B. Madsen, and H. M. Nilsen, Phys. Rev. A **64**, 033418 (2001).
[24] D. Dimitrovski, E. A. Solov'ev, and J. S. Briggs, Phys. Rev. Lett. **93**, 083003 (2004).
[25] H. R. Reiss and N. Hatzilambrou, J. Mod. Opt. **53**, 221 (2006).
[26] D. G. Arbó, E. Persson, and J. Burgdorfer, Phys. Rev. A **74**, 063407 (2006).
[27] P. B. Lerner, K. LaGattuta, and J. S. Cohen, Phys. Rev. A **50**, 3245 (1994).
[28] M. Dörr, Opt. Express **6**, 111 (2000).
[29] G. L. Kamta and A. F. Starace, Phys. Rev. A **68**, 043413 (2003).
[30] E. Goulielmakis *et al.*, Science **320**, 1614 (2008).
[31] T. Tanaka, Phys. Rev. Lett. **114**, 044801 (2015).
[32] T. Balciunas *et al.*, Nat. Comm. **6**, 6117 (2015).